Grey-box modelling and virtual sensors enabling continuous commissioning of hydronic floor heating

Sarran, Lucile; Smith, Kevin M.; Hviid, Christian A.; Rode, Carsten

Published in:
Energy

Link to article, DOI:
10.1016/j.energy.2022.125282

Publication date:
2022

Document Version
Publisher's PDF, also known as Version of record

Energy 261 (2022) 125282

Contents lists available at ScienceDirect

Energy

journal homepage: www.elsevier.com/locate/energy

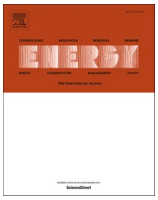

Grey-box modelling and virtual sensors enabling continuous commissioning of hydronic floor heating

Lucile Sarran [a,b], Kevin M. Smith [a,*], Christian A. Hviid [a], Carsten Rode [a,c]

[a] Department of Civil and Mechanical Engineering, Technical University of Denmark, Building 118, Brovej, 2800 Kongens Lyngby, Denmark
[b] Saint-Gobain Nordic A/S, Robert Jacobsens Vej 62A, 2300 Copenhagen, Denmark
[c] Department of Environmental Engineering, Technical University of Denmark, Building 118, Brovej, 2800 Kongens Lyngby, Denmark

ARTICLE INFO

Keywords:
Fault detection and diagnosis
Virtual sensor
Grey-box modelling
Floor heating
District heating

ABSTRACT

Operating district heating systems with low supply and return temperatures improves heat production and distribution efficiency, permitting greater integration of renewable heat sources. Low-temperature district heating is viable without compromising comfort, but faults in end-users' heating systems constrain temperature reductions. Such faults include malfunctioning valves, improper hydronic balancing, and excessive supply temperature setpoints. Occupants lack the resources to detect and diagnose these faults, so there is a need for automated solutions without requiring additional hardware. This paper proposes a method for improving the operation of an apartment's hydronic floor heating system using data from room thermostats, a heat meter and a circulation pump to identify a grey-box model of the system. The resulting model virtually senses each room loop's heat flux, flow, return temperature, and flow coefficient. The authors tested the model on a low-energy apartment in Denmark, using it to diagnose causes of high return temperatures, including poor hydronic balancing and an excessive supply temperature setpoint and pump setting. The authors also used the model to predict the minimum permissible supply temperature maintaining comfort, yielding a reduction in the energy-weighted supply and return temperatures of 8.6 °C and 6.5 °C, respectively.

1. Introduction and background

1.1. Towards a low-carbon heating sector

In 2020, the European Commission proposed a legally binding target of net-zero greenhouse gas emissions by 2050 [1]. As of 2018, fossil fuels still supplied 63% of the European residential heat demand [2]. Heat pumps [3] and district heating (DH) provide cost-effective alternatives that enable the integration of renewable energy sources and excess heat [4]. Thus, Europe can cost-effectively approach its emission goals by increasing the use of district heating rather than only relying on electrification [5].

The typical operating temperatures of DH networks are roughly 85/45 °C [6] (indicating supply and return temperatures of 85 °C and 45 °C, respectively). Scholars have proposed a 4th Generation District Heating with temperatures as low as 50/20 °C, permitting greater integration of large scale heat pumps, solar thermal collectors, and low-temperature heat sources while decreasing distribution heat losses [7–11]. Thus, DH operators can reduce their primary energy consumption by decreasing network temperatures [7–9]. A transition to low-temperature district heating (LTDH) would be highly cost-effective [12,13]. Lund et al. estimated that for every 1 euro invested in decreasing heating system temperatures, district heating investment and operation costs would decrease by 4 euros [14]. Such efforts are not limited to district heating. Lowered temperatures also improve the heating efficiency and capacity in buildings served by local heat pumps, expanding its relevance and application [15].

Several full-scale research projects have demonstrated the benefits of LTDH. A Danish demonstration project reduced the DH supply temperatures for 123 homes in three locations to 50 °C, 55 °C, and 61–66 °C while refurbishing the pipes and heating systems, leading to 63–75% lower heat losses [16]. IEA DHC Annex TS1 showcased LTDH in the UK, Germany, Finland, Denmark and Norway and concluded that LTDH is key to integrating renewable and waste energy for heating [4]. Furthermore, several feasibility studies showed the potential to provide thermal comfort with LTDH in both new and existing buildings [17,18], while new low-energy dwellings with floor heating are especially suitable [11].

* Corresponding author. Building 118 Room 202, Brovej, 2800, Kgs. Lyngby, Denmark.
E-mail addresses: lucile.sarran@gmail.com (L. Sarran), kevs@dtu.dk (K.M. Smith), cahv@dtu.dk (C.A. Hviid), crode@dtu.dk (C. Rode).

https://doi.org/10.1016/j.energy.2022.125282
Received 26 January 2022; Received in revised form 5 July 2022; Accepted 24 August 2022
Available online 29 August 2022

1.2. Faults in space heating systems

Research projects have demonstrated the benefits and feasibility of LTDH in central and Northern Europe, but surveys of district heating practitioners have highlighted several barriers [19,20]. Non-technical barriers include the operators' fear of occupant dissatisfaction, which presides over energy efficiency concerns [20] and can lead building operators to increase the space heating supply temperatures in case of complaints ([21] provides an example). As a result, the supply temperatures in space heating systems are often overly conservative or based on outdated best practices [20]. Meanwhile, the presence of faults (e.g., malfunctioning valves and imbalances due to incorrect valve pre-settings) yield excessive flows through heating elements [6]. These high flows decrease heat utilisation, thereby constraining supply temperature reductions and increasing the return temperatures to the DH network. High return temperatures provide unnecessary heat losses from return pipes and ultimately decrease the utilisation of flue gas condensation and excess heat [22].

Faults can occur in nearly all DH substations components, such as heat exchangers, valves, actuators, sensors, pipes and controllers [23]. However, a large number of faults occur in the end-users' space heating systems (representing 60% of the observed faults in a Swedish study [24]), and fixing these faults showed great potential to reduce return temperatures [25]. These faults include poor balancing of the heating circuits giving excessive flows [26], pre-setting errors [20], malfunctioning valves [6,9,27], incorrectly installed valves [28], undersized radiators [27], oversized circulation pumps [29], and too-high supply temperature setpoints [24]. While DH operators typically monitor heat production and distribution infrastructure intently, the monitoring of substations and individual heating systems is usually the responsibility of end-users, who rarely check for faults as extensively [26,30]. Many district heating utilities leave the responsibility of reducing return temperatures to the occupants [26] and levy motivation tariffs based on the energy-weighted return temperature from heating substations [31]. However, not all customers understand the purpose and implications of such incentive schemes [32]. If the occupants are responsible for detecting faults in heating systems, the faults may persist, obstructing the realisation of LTDH.

1.3. Automated fault detection and diagnosis

A monitoring system could automatically detect and diagnose the faults constraining lower heating temperatures. Automated fault detection and diagnosis (FDD) is a growing and promising field of research, and faulty operation of building systems is a major cause of the energy performance gap [33–35]. However, detecting and diagnosing faults in residences is still largely manual during commissioning and operation [36]. In residential buildings, occupants typically detect faults when they experience discomfort, but they rarely diagnose the cause of faults. Meanwhile, many faults affect system performance but not comfort, so they persist undetected [37]. The growth in collected operational data, whether for control or visualization, makes automated FDD methods increasingly relevant and viable. Detecting and correcting faults before occupants experience discomfort would increase satisfaction, reduce energy consumption and maintenance costs, and ultimately benefit the entire HVAC value chain [37].

In a 2005 review, Katipamula and Brambley [36] described the different stages of the FDD process: fault detection (monitoring a system to detect abnormal operation), fault isolation (determining the type, location and timing of the fault), and fault identification (determining the magnitude and behaviour of the fault). The latter two stages are often carried out together and termed 'fault diagnosis'. Detecting and diagnosing faults continuously, as in ongoing commissioning [38], can use a model of a building's operating conditions with constant updates from measurement data. FDD methods fall into three categories [39,40], which compare the expected and observed operation:

- **Knowledge-based ('white-box') methods**, using a priori physical knowledge to construct a set of rules and thresholds or a physical model of the system.
- **Data-driven ('black-box') methods**, using statistical models based on large datasets. Examples include supervised learning (e.g., regression or classification) [41] and unsupervised learning [41,42].
- **Grey-box methods**, using operational data to calibrate a physical model of the system – i.e., adjusting model parameters to minimise the discrepancy between modelled and measured variables. The inclusion of physical knowledge reduces the number of parameters and improves their validity [43]. However, these models often yield lower predictive accuracy than data-driven models [44,45]. Grey-box models are often used in HVAC system modelling [44,46,47] for predictive control [46–48].

Virtual (or 'soft') sensors use a model to estimate variables when actual sensing is expensive or unreliable, permitting detection of deviations from expected operating conditions [49,50]. Researchers have used virtual sensors to detect faults in air handling units for air conditioning [38,40,51], heat pumps [52] or ventilation systems [53]. Li et al. [49] recommended validating virtual sensors experimentally against physical sensors; however, physical sensors may be impractical or cost-prohibitive. With grey-box methods, the modelling error between modelled and measured variables indicates the reliability of model parameters and virtual sensors [38,46].

1.4. Automated FDD in residential hydronic heating systems

Commercial building operators have incentives to conserve energy and can typically log their operational data, so they are increasingly applying FDD algorithms to continuous commissioning [41,42]. Conversely, residential heating systems operators rarely access detailed data and apply FDD algorithms [6,54,55], requiring new approaches. Fault detection in DH networks have mainly focused on DH substations using heat metering data [23,30,55–59]. These methods detect temperature faults in DH substations but rarely identify their origins, which may occur in the end-users' heating systems [60]. In a simulation study, Brès et al. [60] developed a fault detection algorithm using temperature and flowrate measurements from DH substations. Measuring the supply and return temperatures on the end-user's side significantly improved the algorithm's accuracy. The only example using actual data from end-users' hydronic heating systems is from Østergaard et al. [28], who developed a knowledge-based fault detection method using indoor air temperatures, heat cost allocator data and a thermal radiator model. Although it showed robustness issues, the method successfully detected radiator malfunctions leading to large return temperatures. To the authors' knowledge, no other researchers have developed automated FDD methods for continuous commissioning of hydronic floor heating systems, so this paper addresses the research gap.

1.5. Novelty and objectives

Existing methods detect temperature faults in DH substations, but they do not detect and diagnose faults on the end-users' side of DH networks, likely due to insufficient data [54]. The increasing digitalisation of heat meters and room thermostats provides new data sources on the end-user's side. Programmable thermostats can provide room temperatures and setpoints, while 'smart' heat meters can provide supply and return temperatures and flowrates. Researchers are starting to explore the immense potential of using these data sources to study occupant energy-related behaviour [61–64], energy flexibility [65,66], and automated control of residential heating systems [67,68], among other applications. However, the potential to ensure the low-temperature operation of digitalised residential hydronic heating systems remains largely unfulfilled. Therefore, this article proposes a method using commonly available data sources in new dwellings to

achieve the following:

1. Diagnose faults that prevent lower system temperatures in residential hydronic floor heating systems;
2. Evaluate the extent to which these temperatures can be reduced without affecting occupant comfort;
3. Suggest concrete improvement measures to reduce system temperatures.

The proposed and tested method fits readily available data to a grey-box model of a heating system. Virtual sensors estimate the heat fluxes, flow, return temperatures, and flow coefficients in each room's floor heating loop, indicating any faulty hydronic balancing or high return temperatures. The grey-box method enables simulations with improved hydronic balance and lower supply temperatures to quantitatively indicate the impact of improvements while maintaining thermal comfort. The method does not require detailed physical properties of the building or heating system, yet it offers FDD and targeted operational advice. Overall, the research aims to provide a validated grey-box method for continuously commissioning digitalised hydronic floor heating systems in new residences.

2. Proposed grey-box method

The proposed method uses readily available data from an apartment's hydronic floor heating system to estimate parameters in a grey-box model, with the aim of using these parameters and virtually sensed variables for fault detection and diagnosis. Fig. 1 shows a schematic of the entire modelling process, including parameter estimation.

Section 2.1 describes the physical modelling of a hydronic heating systems in the equation-based Modelica language [69] in the simulation environment Dymola. The model uses differential equations to describe the physical behaviour of virtually sensed variables (inferred) and input/output variables (measured). Section 2.2 describes how the grey-box method iteratively estimates the model parameters to reduce the difference (or residual) between modelled and measured variables. Section 2.3 proposes general steps for detecting faults and improving operation using the grey-box model and virtually sensed variables.

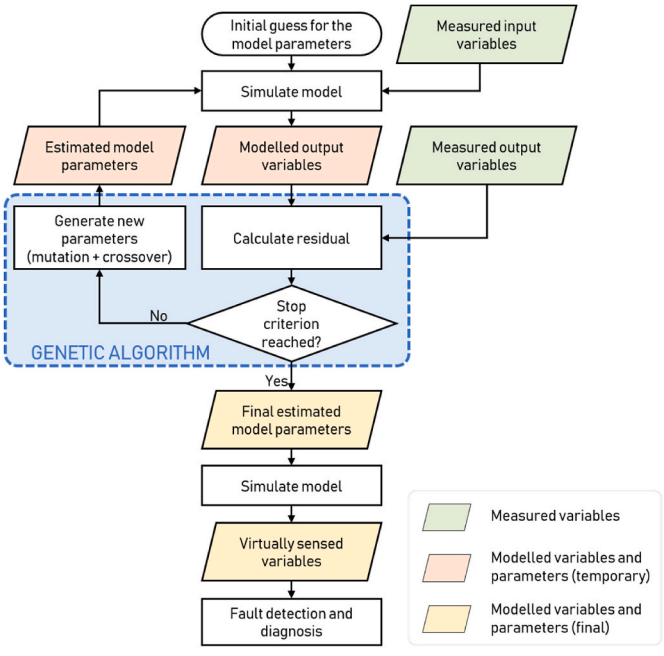

Fig. 1. Schematic of the full modelling process.

2.1. Modelling of hydronic heating

Our proposed approach models the heating system using the equation-based Modelica language using the software Dymola. The physical equations describe the following pressure-flow dependencies of the fluid.

Pressure loss in a horizontal section of pipe is composed of frictional losses Δp_f due to pipe roughness and local losses Δp_l due to e.g. bends and valves. In cylindrical pipes with a constant diameter, the Darcy–Weisbach equation expresses the frictional losses Δp_f, reformulated in Eq. (1):

$$\Delta p_f = f \frac{L}{2D\Delta\rho\Delta A^2}\dot{m}^2 \tag{1}$$

where f is the Darcy friction factor, ρ the density of the water in kg/m^3, L the pipe length in m, D the pipe diameter in m, A the pipe cross-section in m^2, and $\dot{m}$ the mass flowrate in kg/s. The Darcy friction factor depends on the pipe roughness and the Reynolds number, which varies with the fluid velocity.

Eq. (2) expresses the local losses Δp_l (caused by, e.g., valves) as:

$$\Delta p_l = \left(\frac{\dot{m}}{K_v}\right)^2 \tag{2}$$

where $\dot{m}$ is the water mass flowrate, and K_v is the valve's flow coefficient, given by manufacturers as the mass flowrate under a pressure difference of 1 bar.

The developed method should apply to relatively unknown pipes systems, so we assume a constant Darcy friction factor. Eq. (3) expresses the combined frictional and local pressure losses Δp in a section of pipe as:

$$\Delta p = \Delta p_f + \Delta p_l = \left(\frac{\dot{m}}{K}\right)^2 \tag{3}$$

where $\dot{m}$ is the mass flowrate, and K is the equivalent flow coefficient, representing the circulating mass flowrate under a pressure difference of 1 bar.

The proposed method estimates the flow coefficients K and other (assumed constant) unknown parameters in the model of the hydronic heating system. The method aims to use the estimated flow coefficient to guide hydronic balancing and the selection of setpoints for pumps and thermostatic devices.

2.2. Parameter estimation and genetic algorithm

In the proposed grey-box modelling approach, input and output variables are both essentially 'inputs' in the parameter estimation process. That is, a genetic algorithm iteratively evaluates the model fitness by comparing the error between the model variables and the measured data while updating the model parameters. Once the parameters are sufficiently accurate (i.e. considered to have low enough residual), the calibrated grey-box model can simulate and provide 'virtually sensed' variables for fault detection and diagnosis.

The open-source Python tool ModestPy, developed by Arendt et al. [75], iteratively launches simulations and retrieves results while estimating parameters using a genetic algorithm (GA). The tool simulates an imported model as a Functional Mock-Up Unit (FMU). The Functional Mock-up Interface (FMI) is a free standard for exchanging dynamic models (the FMUs) between software [74]. As input, ModestPy accepts an FMU, measured input and output variables, initial guesses, upper and lower bounds, and known parameters. The cost function of the genetic algorithm is the total Normalised Root Mean Square Error (NRMSE):

$$NRMSE_{total} = \sum_i \frac{RMSE_i}{\max(\hat{Y}_i) - \min(\hat{Y}_i)} \tag{4}$$

where:

$$RMSE_i = \sqrt{\frac{\sum_{t=1}^{N}(\hat{Y}_i(t) - Y_i(t))^2}{N}} \quad (5)$$

The index i represents the output variables of the model (e.g., return riser temperature, metered flow, and pump current), N is the number of time steps, and $\hat{Y}_i(t)$ and $Y_i(t)$ are the measured and modelled values of the variable i at time step t, respectively. The algorithm stops when the decrease in NRMSE is below a threshold (e.g., 0.001) for a consecutive number of generations (e.g., 10) or after reaching the maximum number of generations.

2.3. Fault detection, diagnosis, and improvement

Simulating the calibrated grey-box model provides virtually sensed variables in each room loop (e.g., flowrates, supply/return temperatures, and heat supply). We propose the following processes for diagnosis and improvement, which can be iterative:

1. **Analysing the virtual sensor data to detect faults,** such as constant flows or suboptimal valve pre-settings leading to poor hydronic balance, causing high flows and return temperatures from specific loops.
2. **Simulate the grey-box model with realistically improved parameters,** such as lower supply temperature setpoints and improved hydronic balancing, to configure the system with greater overall efficiency while meeting the demands for comfort. Aggregating the heat demand of adjacent rooms may be warranted in some cases, for example, if the heater in a room with a high temperature setpoint consistently heats adjacent zones with lower setpoints, as this should not constrain more efficient operation.

3. Application to a modern apartment

Section 3.1 describes a case study apartment with hydronic floor heating where the authors tested the proposed method using data from the heating system and local heat meter. Section 3.2 describes the model representation of the floor heating system in Dymola and the parameter estimation procedure using ModestPy. Section 3.3 describes the analytical method applied to the case study apartment using the estimated parameters and virtually sensed variables to predict the impact of hydronic balancing and supply temperature reduction.

3.1. Description of the test apartment and collected data

The apartment is in a DGNB-Gold-certified, multi-family apartment building in Copenhagen, Denmark. Constructed in 2017, it has a design primary energy demand of 20.2 kWh/m^2/year. Its external walls and windows have design U-values of 0.12 W/m^{2}K and 0.95 W/m^{2}K, respectively. Fig. 2 shows the façade and 85 m^2 floorplan of the test apartment.

District heating supplies the hydronic floor heating system in all apartments. Each set of supply and return risers distributes heat to six apartments. The kitchen/living room has two parallel floor heating circuits while all other rooms have one. Fig. 3 shows the system in each apartment, modelled in the present work, including the measured and virtually-sensed variables.

A centrifugal pump circulates water through a manifold containing open-close valves. Wall-mounted sensors measure each room temperature, and each valve opens when the room temperature falls below the desired setpoint. The risers also supply radiators on the ground floor, demanding a relatively high temperature compared to the recommended maximum for floor heating systems (due to the risk of thermal discomfort [71] and damage to wooden floors [72]). Therefore, a mixing shunt recirculates a share of the return water to reduce the 'mixed supply temperature' through the floors. A motorised valve controls this temperature according to its setpoint, which the commissioning documents specified should not exceed 35 °C. The heat meter measures the flowrate and supply and return temperatures for water exchanged with the risers, computing the heat output.

Fig. 3 shows the modelling data from the room thermostats, heat meter and circulation pump. Table 1 presents the model input and output variables. The Status Control Value (SCV) is a boolean variable indicating each room's open-close valve status. The gathered dataset included the SCVs, but one could otherwise estimate their values by comparing each room's air temperature and heating setpoint.

3.2. Grey-box modelling of the hydronic heating system

Fig. 4 shows the hydronic floor heating system modelled in the software Dymola.

The model did not include the bathroom and toilet loops, as these were never active during the data collection period. Occupants typically maintain higher air temperature setpoints in these rooms [21], but their heat transfer coefficient is often higher due to tiled floors, yielding an uncertain effect on return temperatures. Henceforth, 'all rooms' or 'the

Fig. 2. South-West façade of the building (left, source: [70]) and floor plan of the test apartment (right).

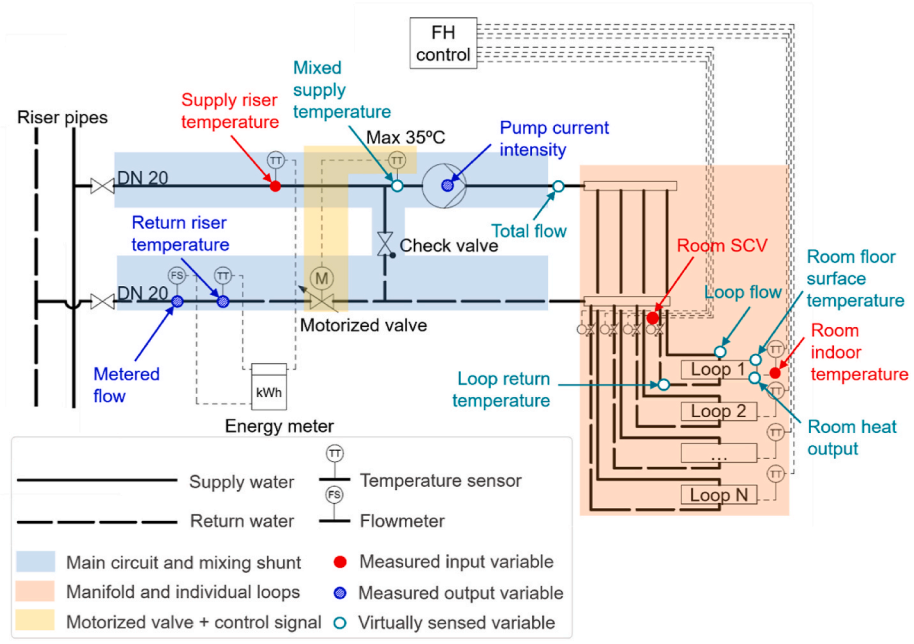

Fig. 3. Schematic of the modelled heating system with measured and virtually sensed variables.

Table 1
Measured data used as model inputs and outputs.

Variable	Description	Data granularity	Input/output of model
T_supply	Supply riser temperature (°C)	5 min	Input
T_roomX	Indoor temperature in Room X (°C)	5 min and at changes >0.5 °C	Input
SCV_roomX	Heating loop valve status in Room X	1 min and at changes	Input
T_return	Return riser temperature (°C)	5 min	Output
metered_flow	Water mass flow from riser (kg/s)	5 min	Output
current	Current drawn by the pump (A)	5 min	Output

entire apartment' refers to the kitchen/living room and Rooms 1, 2 and 3.

The following describes the model of the heating system:

1. **Main circuit and mixing shunt (blue in Figs. 3 and 4).** The authors modelled the supply and return risers as a fluid source and sink, respectively, and provided the measured supply riser temperature as an input. Riser pipes are often oversized, limiting their pressure losses, so the model assumed a constant pressure difference between the risers, dp_riser. A centrifugal pump of type Grundfos Alpha 2 L 15–60 circulates flow in the apartment, so the pump's characteristic curves in Dymola related the flowrate to the pressure head and pump power. The mixing shunt's flow coefficient, K_checkvalve, depends on the unknown pipe diameter and check valve (CV) tuning, so the authors identified its value using parameter estimation.
2. **Manifolds and individual loops (orange in Figs. 3 and 4).** The model assumed a simple flow distributor with no pressure loss for the supply manifold and a small mixing volume for the return manifold. The actual manifolds have poor thermal insulation, exchanging heat with the surrounding air (in the technical closet in the kitchen) and between manifolds. In the model, we connected the heat port of the return manifold (mixing volume) to the kitchen air temperature and supply riser temperature via similar parallel thermal resistances. In periods without heat demand, these resistances governed the rate of heat loss and the decrease in return riser temperatures. The authors estimated relatively high initial resistances and decreased their values until the measured and modelled return riser temperatures matched during periods without heat demand based on visual inspection of the time series data. Each room loop contains a floor heating ('radiant slab') component from the open-source Modelica Buildings Library's [73], which follows the REHVA floor heating modelling scheme [71]. The authors applied typical values for the pipe spacing (200 mm), material (PEX), and size (DN12). The test building's documentation provided input data for the modelled floor construction: 14 mm wooden floor, 80 mm concrete slab embedding the floor heating pipes, 93 mm insulation ($\lambda = 0.046$ W/mK) and 230 mm concrete deck. The authors assumed a constant temperature of 23 °C below the lowest floor layer to represent the adjacent apartment. A boolean SCV signal fully opened or closed each loop's valve. Each loop's flow coefficient, K_room, depends on the unknown pipe properties and valve tuning, so authors identified their values using parameter estimation.
3. **Motorised valve and control signal (yellow in Figs. 3 and 4).** The system regulated flow through a motorised valve (MV) to obtain the mixed supply temperature setpoint, T_set_mixed. The model assumed a simple proportional controller for the motorised valve due to lack of knowledge about the actual controller. The authors assumed that its temperature setpoint and proportional gain remained constant during the data collection period, using parameter estimation for these values and the combined flow coefficient of the return pipe and motorised valve, K_motorvalve.

Table 2 summarises the estimated parameters, including their assumed bounds. Manufacturer data sheets provided the basis for the initial guess and bounds of the valve flow coefficients. In contrast, the estimation bounds for the flow coefficients in each room were deliberately broad to detect poor hydronic balancing.

Table 3 shows the main parameters of the genetic algorithm. The methods applied to the test apartment used data from December 30th' 2018 to January 30th' 2019. The genetic algorithm ran five times with the same initial population (initial guess of the model parameters). The mutation and crossover steps can give different generations, increasing the chance of reaching the global optimum. The authors trained and

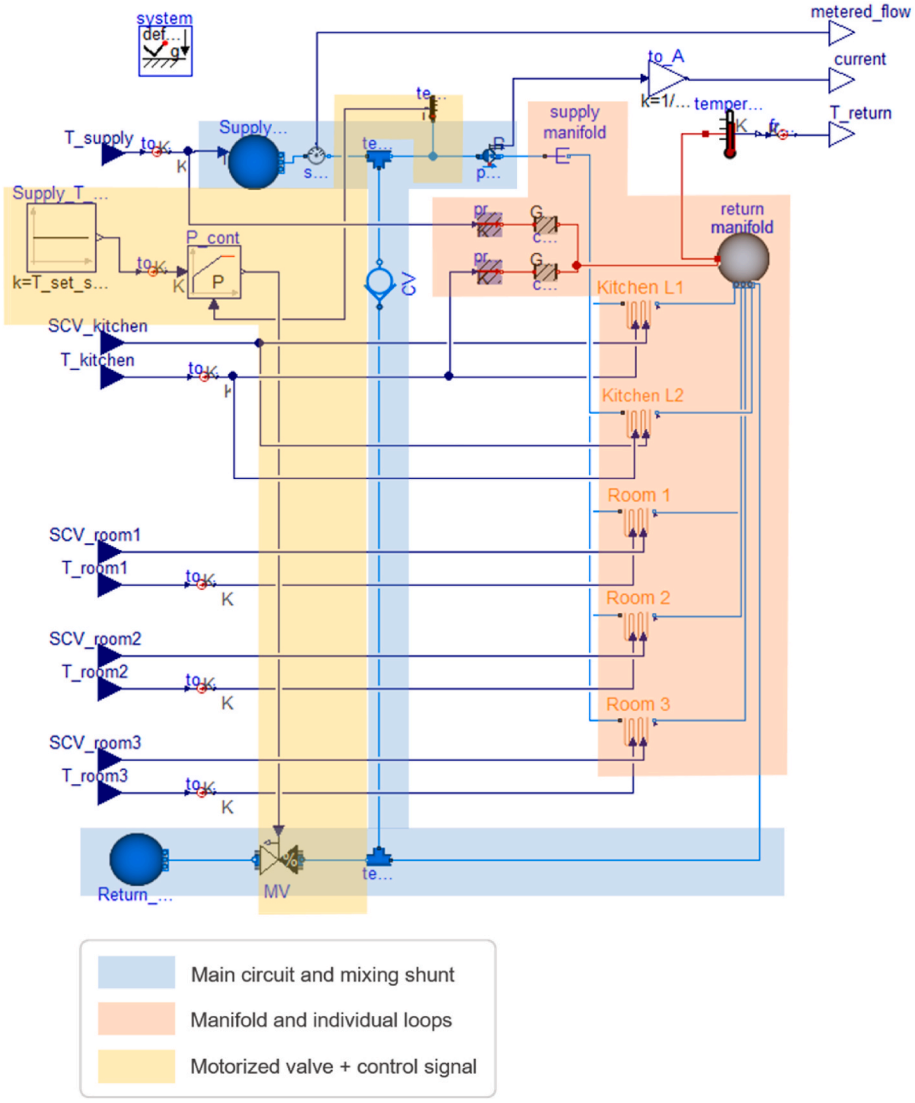

Fig. 4. Apartment heating system modelled in Dymola.

Table 2
Model parameters estimated in the grey-box model.

Parameter	Description	Unit	Estimation bounds: [guess; min; max]
K_checkvalve	Flow coefficient of shunt	kg/s at 1 bar	[2.2; 0.4; 7.0]
K_motorvalve	Flow coefficient of return pipe	kg/s at 1 bar	[0.6; 0.4; 1.4]
K_kitchen	Flow coefficient of each kitchen loop	kg/s at 1 bar	[0.18; 0.07; 10]
K_room1	Flow coefficient of Room 1 loop	kg/s at 1 bar	[0.18; 0.07; 10]
K_room2	Flow coefficient of Room 2 loop	kg/s at 1 bar	[0.18; 0.07; 10]
K_room3	Flow coefficient of Room 3 loop	kg/s at 1 bar	[0.18; 0.07; 10]
gain	Proportional gain of the MV controller	–	[0.15; 0.1; 0.25]
T_set_mixed	Mixed supply temperature setpoint	°C	[45; 32; 50]
dp_riser	Riser differential pressure	Pa	[10,000; 0; 40,000]

validated the model using a 14-day period and subsequent 17-day period, respectively. The best of five runs (smallest NRMSE) yielded the estimated parameters.

Table 3
Parameters of the genetic algorithm.

Simulation parameter	Value
Learning period	14 days
Validation period	17 days
Max. number of generations	40
Population size per generation	50
Tournament size	7
Mutation rate	0.01

3.3. Diagnosis and improvement protocol

The authors ran the calibrated grey-box model using the best-estimated parameters to compute the virtually sensed variables (indicated in Fig. 3), offering a virtual heat meter for each room loop (including flowrates, supply/return temperatures, and heat supply). The diagnosis and improvement procedure occurred in three phases:

1. **Inspecting the virtual sensor data to detect faults.** Section 4.2 compares the virtual sensors' time-series data to best practice values from industry guidelines and design values from the building's

documentation to detect hydronic imbalances (i.e., faulty pre-settings).

2. **Lowering the mixed supply temperature setpoint with the existing hydronic balance.** Section 4.3 presents the feasibility of reducing the mixed supply temperature setpoint without changing the hydronic balance. Simulating the model with constant flow through each room loop (i.e. valves always open) and a lowered mixed supply temperature setpoint yields a corresponding maximum obtainable heat output in each room. We compared these obtainable heat outputs to the original heat demands to identify the lowest suitable setpoint that maintains the same heat output.
3. **Lowering the mixed supply temperature setpoint after improving the hydronic balance.** Section 4.4 presents our model-based approach for adjusting the flows to improve the hydronic balance – e.g., by adjusting the circulation pump setting or the individual loop pre-settings on the control valves [76]. A proper hydronic balance is necessary to achieve low return temperatures in systems supplied by district heating or heat pumps [77]. The balancing strategy included the second step above, minimising the mixed supply temperature setpoint while satisfying the heat demand. The results in all cases focused on the return riser temperatures.

The measured supply riser temperature often decreased due to heat loss when there was no active flow, corresponding to periods where the measured SCV values for all loops were equal to zero (all valves closed). When simulating scenarios with constantly open loop valves, we applied a 3-h moving average to the supply riser temperature and maintained the last value when there was no active flow (i.e., the average supply riser temperature over the 3 h before the drop in flow). Fig. 5 shows the original and transformed time-series data for the supply riser temperature.

4. Results

4.1. Estimated parameters

The five parameter estimation runs (described in Section 3.2) yielded the model with the lowest total NRMSE. Each estimation runs calculated the NRMSE of the three output variables by dividing the RMSEs by the means of the measured data series. The total NRMSE was the sum of the three output variables' NRMSEs. Table 4 presents each NRMSE for the model with the lowest total. The return temperature was the variable with the highest NRMSE, contributing the most to the cost function, but the parameter estimation process could not achieve a lower error.

Table 5 shows the final parameters and total NRMSE.

The listed flow coefficient for the kitchen/living room is for one of its two identical loops. Therefore, the room's total flow coefficient is double its estimated value, K_kitchen. The grey-box method estimated comparable flow coefficients in all three bedrooms. The estimated riser differential pressure was relatively low at only 2 kPa. The estimated flow coefficient K_motorvalve connecting the return manifold to the return riser was much lower than the shunt loop K_checkvalve, implying a high share of recirculation. The estimated mixed supply temperature setpoint was 45.6 °C, much higher than the design value of 35 °C. However, it was realistic considering the measured return riser temperature reached as high as 42 °C.

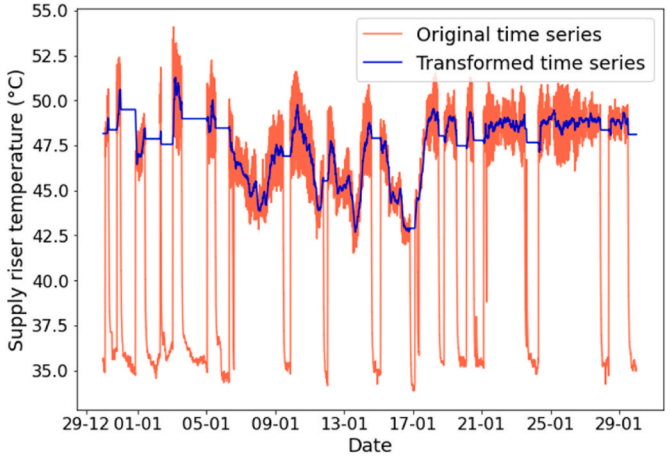

Fig. 5. Supply riser temperature data transformation.

Table 4
NRMSE of each output variable for the model with the lowest total NRMSE.

Variable	NRMSE
T_return	0.084
flow_partial	0.037
current	0.050
TOTAL	**0.171**

Table 5
Estimated parameters.

Parameter	Unit	Estimated value
K_checkvalve	kg/s at 1 bar	2.88
K_motorvalve		0.44
K_kitchen		0.17
K_room1		0.22
K_room2		0.20
K_room3		0.22
dp_riser	Pa	2051
gain	–	0.18
T_set_mixed	°C	45.6
NRMSE		**0.171**

Fig. 6 compares the calibrated model with the corresponding measured data. The model accurately represented the metered flow and pump current but underestimated the return riser temperature. The bias was roughly −3 °C at a maximum, and the difference between measured and modelled energy-weighted return riser temperatures was −1.4 °C for the entire period. The authors could not reduce the bias without harming the accuracy of the other two output variables while staying within the estimation bounds. Section 5 discusses the consequences of this error. The model acceptably represented the metered flow and pump current (directly linked to the total flow through the floor loops), enabling an evaluation of the system's hydronic balance.

4.2. Fault diagnosis comparing virtually sensed variables to expected values

Fig. 7 shows the virtual sensor data in the four main rooms. The virtually-sensed return temperature in all three bedrooms reached 38–40 °C when the mixed supply temperature was roughly 41 °C, indicating low cooling. The virtually-sensed cooling in Room 3 was the smallest of all rooms. It was rarely more than 1.5 °C, whereas the standard dimensioning assumption is generally 5 °C for floor heating [78]. The return temperature from the kitchen/living room loops was lower than from the other rooms, but it never reached a steady-state before its flow was deactivated.

The virtually-sensed flows in Rooms 1, 2 and 3 were always above 0.1 kg/s, whereas standard dimensioning practice would suggest 0.02 kg/s (based on their design heat loss and supply/return temperatures of 35/30 °C [79]). Each of the bedrooms' floor heating outputs peaked between 400 and 600 W, and their floor surface temperatures reached 27–28 °C – close to the upper comfort limit [71] and slightly above the recommended maximum of 27 °C for wooden floors [72]. When active, the kitchen/living room's floor surface temperature reached 26–28 °C,

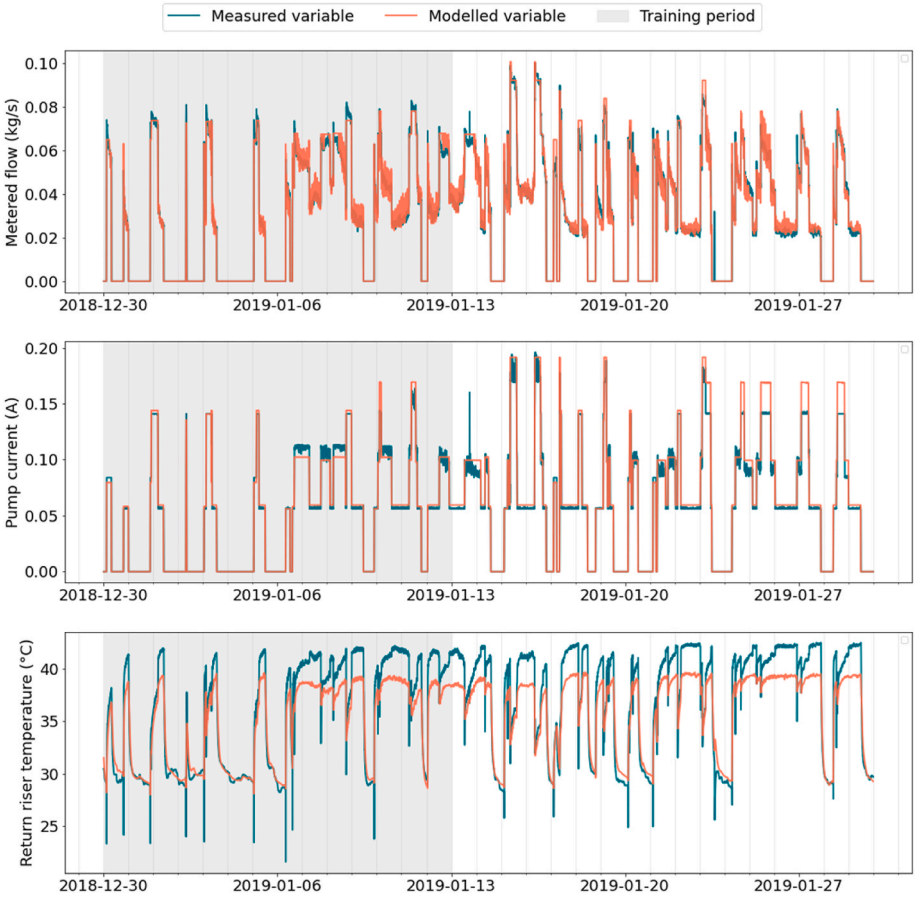

Fig. 6. Measured and modelled output variables of the model.

and each of its loops peaked at 500–700 W.

Table 6compares the virtually-sensed values to the design practice values. This diagnosis depends on the model's accuracy, so the systematic underestimation of the return riser temperature may bias the results (further discussed in Section 5).

4.3. Potential for decreasing the mixed supply temperature setpoint

The estimated mixed supply temperature setpoint (45.6 °C) was substantially higher than the design value (35 °C). Before reducing this setpoint (Section 4.3.2), we must consider whether a high heating intensity was necessary to satisfy abnormal demand (e.g., due to high thermal losses or indoor temperature setpoints) and whether a lower, more stable heating intensity could satisfy the occupants' comfort requirements.

4.3.1. Analysis of heat operation and indoor temperature in the rooms

Fig. 8 shows the measured air temperature, temperature setpoints, and floor heating status in the four main rooms over ten days in the studied period (January 2019). The programmable thermostat decreases the setpoint temporarily in response to rapid decreases in room temperature, so the large drops in the kitchen/living room setpoint are due to window openings.

The mixed supply temperature setpoint yielded a high heating intensity, increasing the air temperature by 1 °C over six to 12 h despite the high thermal lag of the concrete construction. Other than in Room 3, the high heating intensity excessively heated the floors, yielding intervals of 1–2 days between heating periods. Operating the floor heating with lower temperatures would allow shorter intervals between heating periods, providing a more stable delivery with lower peaks.

From January 10th to January 15th, Room 3 and the kitchen/living room had the same indoor temperatures despite having a 1 °C difference in setpoints. The floor heating loop was constantly active in Room 3 and never active in the kitchen/living room during this period. It seems likely that Room 3 heated the adjacent kitchen/living room, perhaps explaining why the heat output in Room 3 sustained roughly 400 W for periods of several days throughout much of January, as Fig. 7 showed.

4.3.2. Decrease in mixed supply temperature setpoint

Fig. 9 compares the results of simulations with lowered mixed supply temperature setpoints and constant flow through all loops (red curves) to the 2-day moving average of the actual heat demand (cyan curve) – two days was roughly the period between open-close cycles. For reference, the figure includes each room's design heat demand at an outdoor temperature of −12 °C with no internal heat gains (black dashed line). Lowering the setpoint could satisfy the demand without compromising comfort in all but Room 3. However, Section 4.3.1 indicated that Room 3 often heated the kitchen/living room. Therefore, limiting Room 3's heat output to its design value would help avoid overheating adjacent rooms, forcing the kitchen/living room to heat itself.

As expected, a mixed supply temperature setpoint of 35 °C to 37 °C could satisfy the design heat demand in each room, which was consistent with the construction documents (35 °C). Moreover, a supply temperature of 33 °C or less could satisfy the actual heat demand in the kitchen/living room. However, the peaks in actual demand in all three bedrooms exceeded the design value, requiring supply temperatures of 37 °C, 40 °C, and more than 45.6 °C, respectively. In some cases, the cause for exceeding the design values was unclear, but indoor temperature setpoints exceeding 20 °C (i.e. the design value) could only account for a small share of the increase.

To account for the unintended heating of adjacent rooms, one can combine the rooms' heat demands and repeat the procedure at the

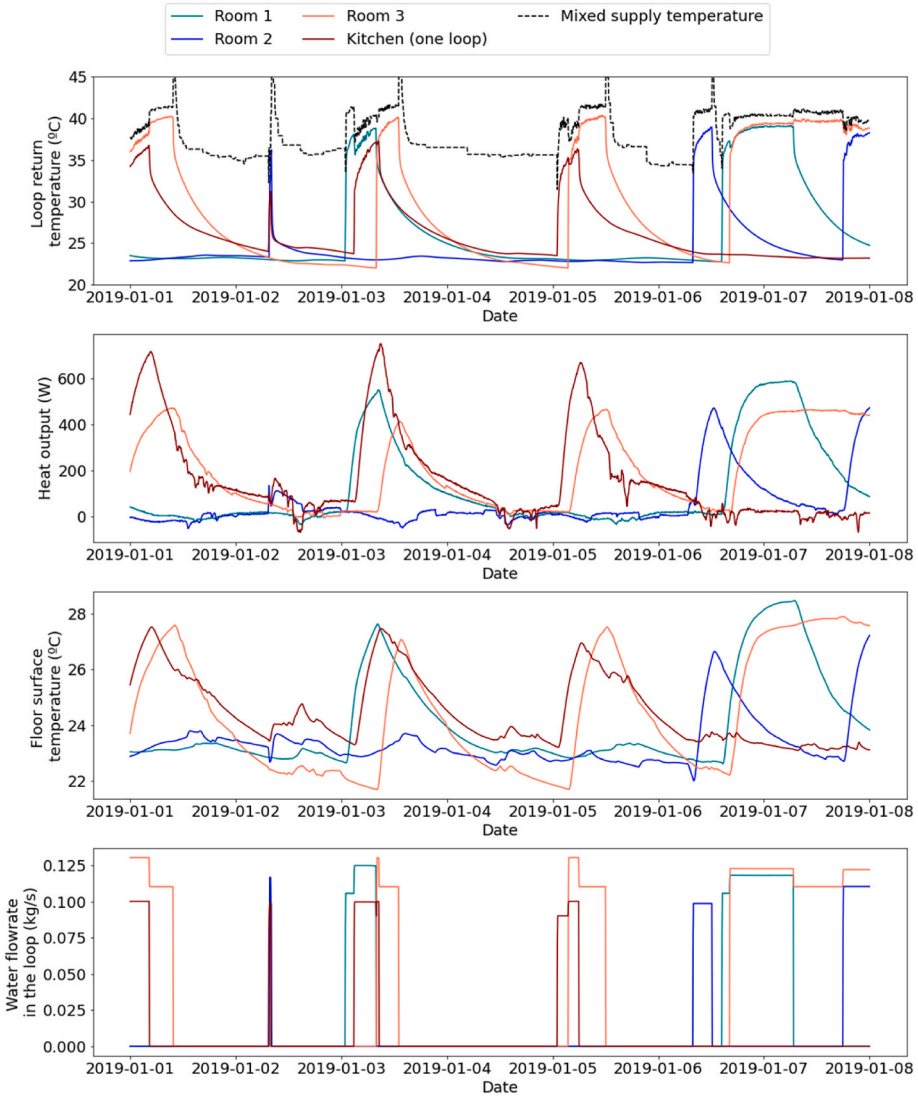

Fig. 7. Times series of the virtually sensed variables.

Table 6
Comparison between estimated variables and best practice.

Variable	Virtually-sensed values	Reference values	Reference source
Mixed supply temp. setpoint	45.6 °C	35 °C	Design values (construction project documentation)
Cooling in the loops	bedrooms: around 2 °C living room: 5 °C	5 °C	Industry guidelines [78]
Water flows in the loops	0.08–0.13 kg/s	0.01–0.03 kg/s	Industry sizing tool [79]
Heat output from the floor	bedrooms: 400–600 W peak, 400 W in avg. when active living room: 500–750 W peak, 360 W in avg. when active	bedrooms: 250–350 W living room: 460 W	Design values (construction project documentation)
Floor temperature	26 to 29 °C	19 to 29 °C for comfort 27 °C for wooden floor	REHVA guidebook [71] Floor manufacturer [72]

apartment scale. Fig. 10 shows that a mixed supply temperature setpoint close to 33 °C and not higher than 35 °C should be sufficient to provide the required heat throughout January, which was the coldest month of the year.

Table 7 shows the energy-weighted and maximum return riser temperatures with lowered mixed supply temperature setpoints. A mixed supply temperature setpoint of 35 °C, as suggested by Fig. 10, could decrease the return riser temperature to 31.3 °C – a reduction of roughly 6 °C from current conditions.

4.4. Additional strategies for return temperature reduction

Table 5 showed that the room loops' virtually-sensed flows were much larger than the recommended design practice. Reducing these flows could provide ideal cooling and reduce the return riser temperature, so the authors investigated the following:

1. **Changing the pump curve.** The pump operated with a proportional relationship between pressure head and flow, but the user could choose between two differently sloped curves. Switching to the curve with the lower pressure head would reduce the flows in all loops.
2. **Balancing the system by decreasing the flow coefficients of specific loops**. Assuming that one could change the pre-settings on

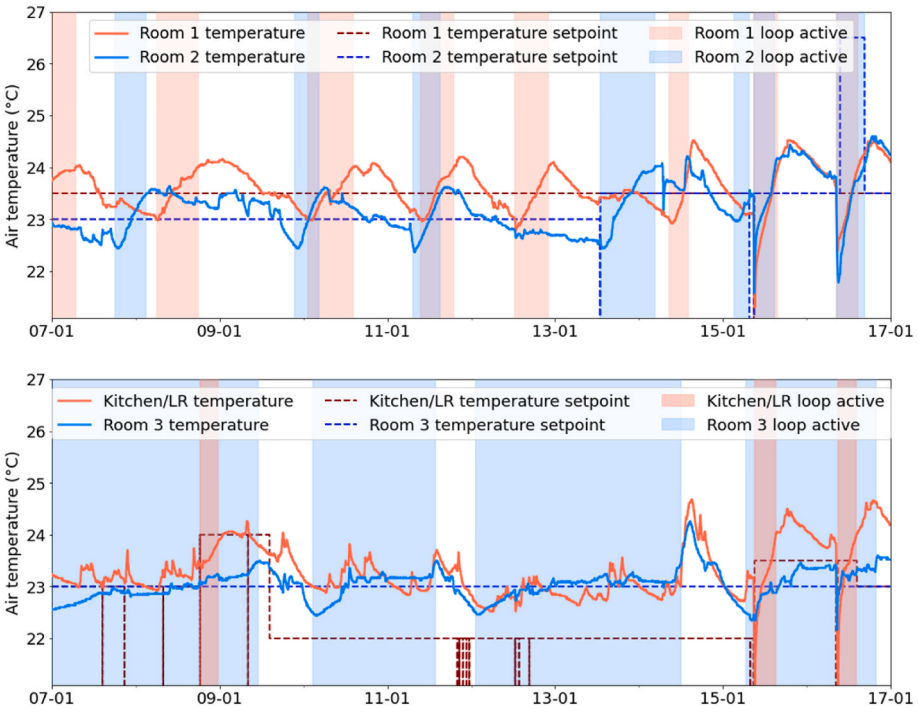

Fig. 8. Indoor air temperature, temperature setpoint and floor heating loop status during ten days in January 2019.

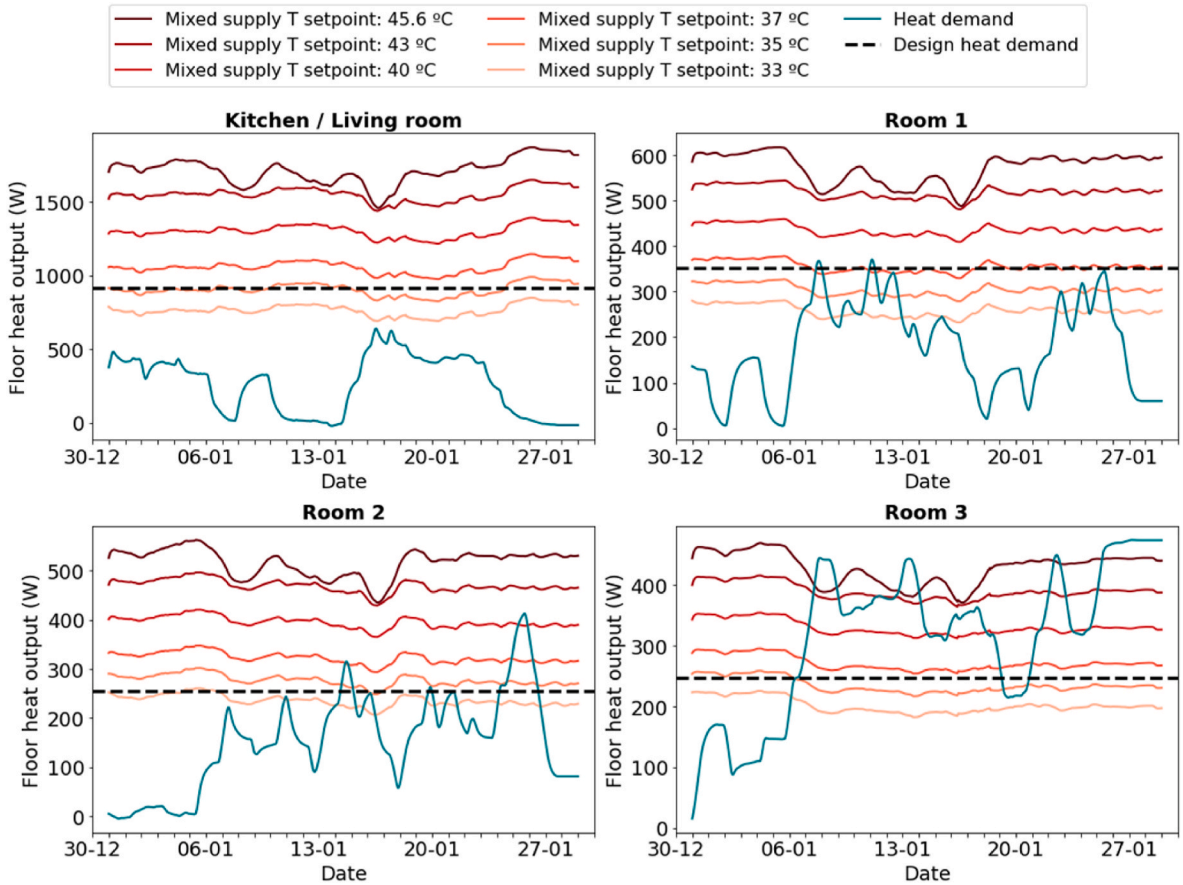

Fig. 9. Modelled heat output delivered with different mixed supply temperature setpoints in each room (with all floor heating loops active), modelled heat demand and design heat demand.

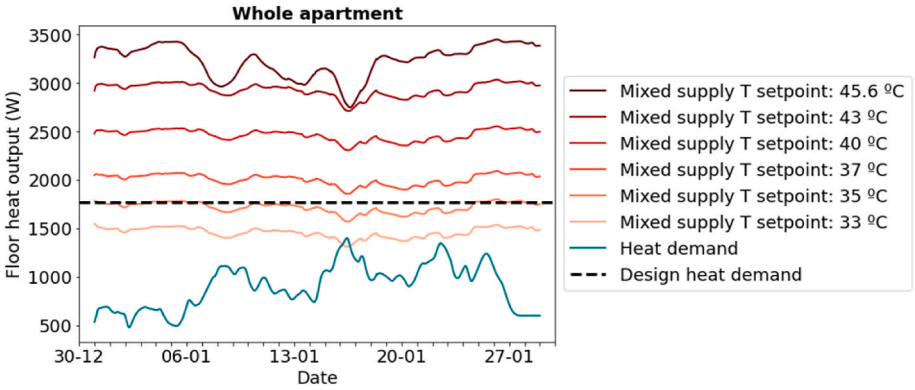

Fig. 10. Modelled heat output delivered with different mixed supply temperature setpoints in the whole apartment (with all floor heating loops active), modelled heat demand and design heat demand.

Table 7
Energy-weighted and maximum return riser temperatures with lowered mixed supply temperature setpoints and all floor heating loops active.

Mixed supply temperature setpoint (°C)	Energy-weighted mean return riser temperature (°C)	Maximum return riser temperature (°C)
45.6	37.5	38.7
43	36.4	36.9
40	34.4	34.9
37	32.5	33.0
35	31.3	31.8
33	30.2	31.5

the return manifold's control valves, one could reduce the flow coefficients of the loops with excessive flows. The authors artificially decreased the flow coefficients and corresponding flows until they matched the suggested values from a dimensioning tool [79]: 0.022 kg/s in each kitchen/living room loop, 0.017 kg/s in Room 1 and 0.012 kg/s in Rooms 2 and 3. Fig. 11 shows the two pump curves and the system curve before and after balancing, and it highlights the operating points in the three scenarios (with all room loops active).

Both scenarios repeated the procedure in Section 4.3: lowered mixed supply temperature setpoints with all floor heating valves open to find the minimum feasible setpoint after aggregating all heat demand. Fig. 12 provides an overview of each scenario's energy-weighted return riser temperature for the entire period.

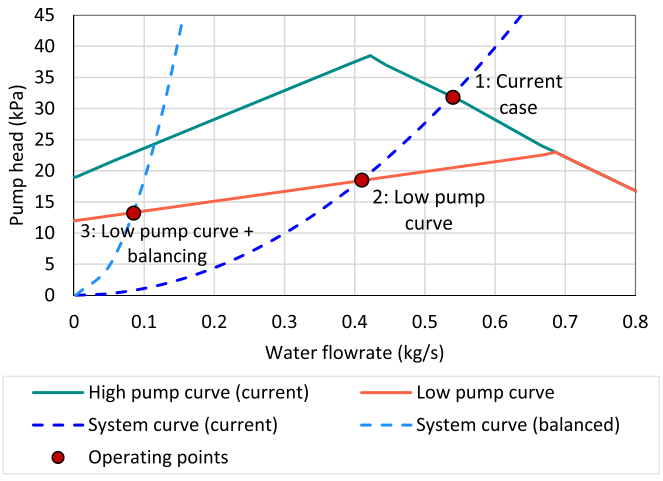

Fig. 11. Pump curves and operating points of the successive improvement scenarios.

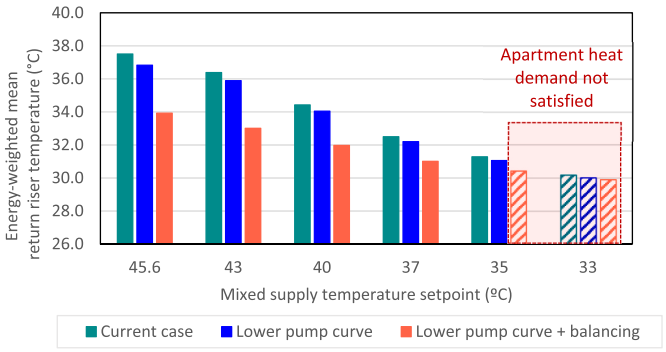

Fig. 12. Energy-weighted mean return riser temperatures in different flow reduction scenarios and with different mixed supply temperature setpoints.

The lower pump curve had a limited impact on the return riser temperature without improving the hydronic balance. Balancing the system significantly reduced the energy-weighted return riser temperature at any mixed supply temperature. Reducing the mixed supply temperature setpoint to 37 °C yielded a return riser temperature of 31 °C, which is 6.5 °C less than the existing system. Surprisingly, after hydronic balancing, the design mixed supply temperature setpoint from the construction documents (35 °C) did not satisfy the apartment's heat demand. However, the model's inability to accurately represent the shunt operation yielded a discrepancy between the mixed supply temperature setpoint and its realised value. For instance, a setpoint of 35 °C did not provide a mixed supply temperature higher than 32.5 °C, which may be too low to satisfy the apartment's heat demand. Section 5 discusses this in more detail.

Moreover, reducing the flows to their design values reduced the required pump power by a factor of three. The position of the new system curve (far left in Fig. 11) indicates that the pump was likely oversized, so perhaps a smaller model could replace it.

Reducing a single apartment's space heating return temperature from 37.5 °C to 31 °C would provide insignificant energy savings on its own. However, a similar result for all apartments would decrease distribution losses and increase heat production efficiencies (e.g., increased flue gas condensation in biomass boilers). Using the performance curves from Ref. [80] for a biomass boiler with a fuel water content of 0.4 kg/kg and a heat exchange efficiency of 85%, we estimate that such a return temperature reduction would lead to a 3% increase in the thermal energy output of the boiler. A more detailed investigation could refine this number, adding the impact of lower distribution heat losses from return pipes and evaluating the benefits of lower supply temperatures, especially for low-temperature heating systems based on renewable energy sources and excess heat.

5. Discussion

The virtual sensors' reliability depended on the model's accuracy. The model needed to ensure a large share of recirculated flow to match the measured pump current and return flow, which reduced the mixed supply and return riser temperatures. The modelled return riser temperature was systematically 1.4 °C lower than was measured. The authors could not eliminate this bias by adjusting the parameters or estimation bounds, likely due to assumptions about the heating system's design and control. Reliable information about the operating conditions could improve the accuracy and reliability. For example, the model combined the measured pump current and modelled pump curve to determine the pump's circulated flow. This proxy required manual specification of the pump curves, adding some uncertainty. Moreover, the grey-box method estimated the shunt's control parameters (i.e., mixed supply temperature setpoint and controller gain), but someone with access to the system and its datasheets could identify these values, limiting the number of estimated parameters. In practice, they could further improve the parameter estimation process by varying the control setpoints to excite the system, thereby expanding the range of operating conditions for training the model. Furthermore, decreasing the mixed supply temperature setpoint before reiterating the grey-box method could improve the model's accuracy in the range of the lower mixed supply temperatures.

The proposed grey-box method uses data from hydronic heating systems, smart heat meters, and smart room thermostats to virtually sense the flows and return temperatures from each room loop – a kind of virtual heat meter for every room. One can compare a room's virtually-sensed heating power to its dimensioned value to detect overuse (e.g., heating adjacent rooms; concurrent heating and ventilative cooling; stuck-open valves). Similarly, one can compare a loop's virtually sensed flows, flow coefficients, or cooling to its dimensioned values to detect poor hydronic balance, informing specific changes to the valve's pre-settings. The grey-box method can also indicate the minimum mixed supply temperatures that satisfy the demand for heating and can readily predict the effect of reducing the pump settings – something building operators often fear.

The virtual sensors indicated that the mixed supply temperature and individual loops' flows were excessive, forcing the system to operate with a high heating power. One could deduce the same findings by inspection. The measured return riser temperature was systematically above 40 °C when at least one loop was active, showing that the mixed supply temperature setpoint was at least 40 °C and likely higher than 42 °C. As Fig. 6 shows, on December 30th, 2018, active heating in only the kitchen/living room yielded a metered flow of roughly 0.06 kg/s, while active heating in only Room 2 yielded a metered flow of roughly 0.03 kg/s. Adding recirculation, the room loops' flows must have been even greater, exceeding their design flows by a sizable margin (according to a dimensioning tool [79]: 0.044 kg/s in the kitchen/living room; 0.017 kg/s in Room 2). A rule-based fault detection and diagnosis algorithm could identify these faults without requiring the proposed grey-box method. However, it would not determine the minimum feasible supply temperature and pump setting while predicting the impact of specific balancing measures on the energy-weighted return temperature.

In addition to the pump data, the grey-box method required the floor area of the different rooms (easy to obtain) and information about the floor construction and pipe layout. However, one may apply averages for a given building type and construction year. Therefore, one could reasonably apply the grey-box method to other buildings. In this study, the authors applied the proprietary software Dymola. However, one could use open-source Modelica-based software to implement the grey-box method.

6. Conclusion

This paper presents a novel grey-box method for detecting and diagnosing operational faults constraining the low-temperature operation of hydronic floor heating systems. The grey-box model requires data from the room thermostats, heat meter, and circulation pump if one exists. It virtually senses the flows, flow coefficients, heat fluxes, and return temperatures in each room loop of the heating system. The authors applied the method to a modern Danish apartment. The identified grey-box model was reasonably accurate concerning the error between the modelled and measured return riser temperatures, metered flows, and pump currents, yielding NRMSE values of 0.084, 0.037, and 0.050 respectively, for a total of 0.171. The return riser temperature was the least accurate of the three variables, giving a systematic error (1.4 °C on average). The virtual sensors indicated excessive supply temperatures and poor hydronic balance, causing high return temperatures and flow rates in each loop. The grey-box model predicted the impact of improvement strategies to reduce these temperatures and flowrates, namely reducing the pump setting, decreasing the mixed supply temperature setpoint, and adjusting the valves' pre-settings to decrease the flow coefficients. These improvement measures reduced the modelled energy-weighted supply and return temperatures by 8.6 °C and 6.5 °C respectively. In addition to improving heat production and distribution efficiency, lowering the system temperatures can help reduce peak loads and unintended heating of adjacent rooms while stabilising indoor temperatures. Occupants and operators could broadly apply such continuous commissioning tools to ensure efficient operation of residential heating systems.

Concerning future work, the grey-box method could become more accurate with knowledge of the mixed supply temperature setpoint and direct measurements of the heating system's total flows. In a system without a local mixing loop in each apartment, the heat meter would provide both values and perhaps also the pressure difference (between supply and return), demanding a simpler model with fewer estimated parameters. The authors are working to establish such models. Ultimately, the grey-box methods could enable an automated service for continuous commissioning of hydronic floor heating systems in modern apartments, guiding operators with precise instructions to optimise performance. Such a tool could minimise the return temperature penalties for end-users and the overall costs for societies' transition to low-temperature district heating based on renewable energy sources.

Credit author statement

Lucile Sarran: Conceptualization, Methodology, Software, Investigation, Writing – Original Draft, Visualization, Kevin Michael Smith: Conceptualization, Methodology, Writing – Review & Editing, Supervision, Christian Anker Hviid: Conceptualization, Writing – Review & Editing, Supervision, Carsten Rode: Conceptualization, Supervision.

Declaration of competing interest

The authors declare that they have no known competing financial interests or personal relationships that could have appeared to influence the work reported in this paper.

Data availability

The authors do not have permission to share data.

Acknowledgements

This work was primarily funded by Saint-Gobain Nordic A/S, the Danish Innovation Fund and Realdania (grant number 7038-00224A). The Danish Innovation Fund also funded the work as part of the HEAT 4.0 project (grant number 8090-00046B). The data used in this study

was collected as part of the EnergyLab Nordhavn project, funded by EUDP (EUDP 64015-0055).

References

[1] European Commission. Committing to climate-neutrality by 2050: commission proposes European climate law and consults on the European climate pact. 2020.
[2] Heating Enerdata. Energy consumption by energy source. Odyssee-Mure Project; 2018. https://www.odyssee-mure.eu/publications/efficiency-by-sector/households/heating-energy-consumption-by-energy-sources.html.
[3] Connolly D, Mathiesen BV. A technical and economic analysis of one potential pathway to a 100% renewable energy system. Int J Sustain Energy Plann Manag 2014;1:7–28. https://doi.org/10.5278/ijsepm.2014.1.2.
[4] Li H, Svendsen S, Gudmundsson O, Kuosa M, Rämä M, Sipilä K, et al. Future low temperature district heating design guidebook: final report of IEA DHC Annex TS1. Low temperature district heating for future energy systems. 2017. https://doi.org/10.1016/j.egypro.2018.08.224.
[5] Connolly D, Lund H, Mathiesen BV, Werner S, Möller B, Persson U, et al. Heat roadmap Europe: combining district heating with heat savings to decarbonise the EU energy system. Energy Pol 2014;65:475–89. https://doi.org/10.1016/j.enpol.2013.10.035.
[6] Østergaard DS. Heating of existing buildings by low-temperature district heating. 2018.
[7] Lund H, Werner S, Wiltshire R, Svendsen S, Thorsen JE, Hvelplund F, et al. 4th Generation District Heating (4GDH). Integrating smart thermal grids into future sustainable energy systems. Energy 2014;68:1–11. https://doi.org/10.1016/j.energy.2014.02.089.
[8] Averfalk H, Werner S. Essential improvements in future district heating systems. Energy Proc 2017;116:217–25. https://doi.org/10.1016/j.egypro.2017.05.069. Elsevier Ltd.
[9] Dalla Rosa A, Li H, Svendsen S, Werner S, Persson U, Ruehling K, et al. IEA DHC Annex X report: toward 4th generation district heating: experience and potential of low-temperature district heating. 2014.
[10] Benakopoulos T, Salenbien R, Vanhoudt D, Svendsen S. Improved control of radiator heating systems with thermostatic radiator valves without pre-setting function. Energies 2019;12. https://doi.org/10.3390/en12173215.
[11] Danish Energy Agency. Guidelines for low-temperature district heating. A deliverable of EUDP 2010-II: full-scale demonstration of low-temperature district heating in existing buildings. 2014.
[12] Ommen T, Markussen WB, Elmegaard B. Lowering district heating temperatures - impact to system performance in current and future Danish energy scenarios. Energy 2016;94:273–91. https://doi.org/10.1016/j.energy.2015.10.063.
[13] Averfalk H, Werner S. Economic benefits of fourth generation district heating. Energy 2020;193. https://doi.org/10.1016/j.energy.2019.116727.
[14] Lund H, Alberg Østergaard P, Chang M, Werner S, Svendsen S, Sorknæs P, et al. The status of 4th generation district heating : research and results. Energy 2018;164:147–59. https://doi.org/10.1016/j.energy.2018.08.206.
[15] Staffell I, Brett D, Brandon N, Hawkes A. A review of domestic heat pumps. Energy Environ Sci 2012;5:9291–306. https://doi.org/10.1039/c2ee22653g.
[16] Danish Energy Agency. EUDP 2010-II Fuldskalademonstration af lavtemperatur-fjernvarme i eksisterende bebyggelser [Full-scale demonstration of low temperature district heating in existing buildings. 2014.
[17] Østergaard DS, Svendsen S. Space heating with ultra-low-temperature district heating - a case study of four single-family houses from the 1980s. Energy Proc 2017;116:226–35. https://doi.org/10.1016/j.egypro.2017.05.070.
[18] Hesaraki A, Holmberg S. Energy performance of low temperature heating systems in five new-built Swedish dwellings: a case study using simulations and on-site measurements. Build Environ 2013;64:85–93. https://doi.org/10.1016/j.buildenv.2013.02.009.
[19] Guzzini A, Pellegrini M, Pelliconi E, Saccani C. Low temperature district heating: an expert opinion survey. Energies 2020;13:810. https://doi.org/10.3390/en13040810.
[20] Averfalk H, Werner S, Felsmann C, Rühling K, Wiltshire R, Svendsen S. Transformation roadmap from high to low temperature district heating systems: Annex XI final report. 2017.
[21] Sarran L, Lex SW, Wærsted EH. Comfort and technical installations in Danish low-energy homes: reconnecting design intention and domestic perceptions. Build Res Inf 2021:1920362. https://doi.org/10.1080/09613218.2021.1920362.
[22] Frederiksen S, Werner S. District heating and cooling. Studentlitteratur AB; 2013. https://doi.org/10.1016/B978-0-12-409548-9.01094-0.
[23] Pakanen J, Hyvärinen J, Kuismin J, Ahonen M. Fault diagnosis methods for district heating substations. 1996.
[24] Zinko H, Hoon L, Bong-Kyun K, Youn-Hong K, Lindkvist H, Loewen A, et al. Improvement of operational temperature differences in district heating systems. In: IEA R&D programme on district heating and cooling. Netherlands Agency for Energy and the Environment; 2005.
[25] Petersson S, Werner S. Long-time properties of low-flow adjusted radiator systems. Laangtidsegenskaper hos laagfloedesinjusterade radiatorsystem; 2003.
[26] Månsson S, Johansson Kallioniemi PO, Thern M, Van Oevelen T, Sernhed K. Faults in district heating customer installations and ways to approach them: experiences from Swedish utilities. Energy 2019;180:163–74. https://doi.org/10.1016/j.energy.2019.04.220.
[27] Østergaard DS, Svendsen S. Experience from a practical test of low-temperature district heating for space heating in five Danish single-family houses from the 1930s. Energy 2018;159:569–78. https://doi.org/10.1016/j.energy.2018.06.142.
[28] Østergaard DS, Paulsen O, Sørensen IB, Svendsen S. Test and evaluation of a method to identify heating system malfunctions by using information from electronic heat cost allocators. Energy Build 2019;184:152–62. https://doi.org/10.1016/j.enbuild.2018.12.004.
[29] Quiquerez L, Santelices C, Daniel J, Hollmuller P, Lachal BM. Températures de distribution de chauffage du parc immobilier genevois. 2013.
[30] Gadd H, Werner S. Fault detection in district heating substations. Appl Energy 2015;157:51–9. https://doi.org/10.1016/j.apenergy.2015.07.061.
[31] Li H, Sun Q, Zhang Q, Wallin F. A review of the pricing mechanisms for district heating systems. Renew Sustain Energy Rev 2015;42:56–65. https://doi.org/10.1016/j.rser.2014.10.003.
[32] Sernhed K, Gåverud H, Sandgren A. Customer perspectives on district heating price models. Int J Sustain Energy Plann Manag 2017;13:47–60. https://doi.org/10.5278/ijsepm.2017.13.4.
[33] de Wilde P. The gap between predicted and measured energy performance of buildings: a framework for investigation. Autom ConStruct 2014;41:40–9. https://doi.org/10.1016/J.AUTCON.2014.02.009.
[34] Roth KW, Westphalen D, Llana P, Feng M. The energy impact of faults in US commercial buildings. In: International refrigeration and air conditioning conference; 2004. p. 665.
[35] Mills E. Building commissioning: a golden opportunity for reducing energy costs and greenhouse gas emissions in the United States. Energy Effic 2011;4:145–73. https://doi.org/10.1007/s12053-011-9116-8.
[36] Katipamula S, Brambley MR. Review article: methods for fault detection, diagnostics, and prognostics for building systems—a review, part I. HVAC R Res 2005;11:3–25. https://doi.org/10.1080/10789669.2005.10391123.
[37] Rogers AP, Guo F, Rasmussen BP. A review of fault detection and diagnosis methods for residential air conditioning systems. Build Environ 2019:106236. https://doi.org/10.1016/J.BUILDENV.2019.106236.
[38] Gunay B, Shen W, Yang C. Characterization of a Building's operation using automation data: a review and case study. Build Environ 2017;118:196–210. https://doi.org/10.1016/j.buildenv.2017.03.035.
[39] Yang H, Zhang T, Li H, Woradechjumroen D, Liu X. HVAC equipment, unitary: fault Detection and diagnosis. In: Encyclopedia of energy engineering and technology. second ed. 2014. p. 854–64. https://doi.org/10.1081/e-eee2-120051345.
[40] Li H, Braun JE. A methodology for diagnosing multiple simultaneous faults in vapor-compression air conditioners. HVAC R Res 2007;13:369–95. https://doi.org/10.1080/10789669.2007.10390959.
[41] Mirnaghi MS, Haghighat F. Fault detection and diagnosis of large-scale HVAC systems in buildings using data-driven methods: a comprehensive review. Energy Build 2020;229:110492. https://doi.org/10.1016/j.enbuild.2020.110492.
[42] Zhao Y, Li T, Zhang X, Zhang C. Artificial intelligence-based fault detection and diagnosis methods for building energy systems: advantages, challenges and the future. Renew Sustain Energy Rev 2019;109:85–101. https://doi.org/10.1016/j.rser.2019.04.021.
[43] Kristensen NR, Madsen H, Jørgensen SB. Parameter estimation in stochastic grey-box models. Automatica 2004;40:225–37. https://doi.org/10.1016/j.automatica.2003.10.001.
[44] Afram A, Janabi-Sharifi F. Black-box modeling of residential HVAC system and comparison of gray-box and black-box modeling methods. Energy Build 2015;94:121–49. https://doi.org/10.1016/j.enbuild.2015.02.045.
[45] Arendt K, Jradi M, Shaker HR, Veje CT. Comparative Analysis of white- , gray- and black-box models for thermal simulation of indoor environment: teaching building case study. In: Building performance modeling conference; 2018. p. 173–80.
[46] Afram A, Janabi-Sharifi F. Gray-box modeling and validation of residential HVAC system for control system design. Appl Energy 2015;137:134–50. https://doi.org/10.1016/j.apenergy.2014.10.026.
[47] Gunay HB, O'Brien W, Beausoleil-Morrison I. Control-oriented inverse modeling of the thermal characteristics in an office. Sci Technol Built Environ 2016;22:586–605. https://doi.org/10.1080/23744731.2016.1175893.
[48] So ATP, Chan WL, Chow TT, Tse WL. New HVAC control by system identification. Build Environ 1995;30:349–57. https://doi.org/10.1016/0360-1323(94)00063-X.
[49] Li H, Yu D, Braun JE. A review of virtual sensing technology and application in building systems. HVAC R Res 2011;17:619–45. https://doi.org/10.1080/10789669.2011.573051.
[50] Ahmad I, Ayub A, Kano M, Cheema II. Gray-box soft sensors in process industry: current practice, and future prospects in era of big data. Processes 2020;8:1–20. https://doi.org/10.3390/pr8020243.
[51] Ahamed MS, Zmeureanu R, Cortrufo N, Candanedo J. Gray-box virtual sensor of the supply air temperature of air handling units. Science and Technology for the Built Environment 2020;26:1151–62. https://doi.org/10.1080/23744731.2020.1785812.
[52] Li H, Braun JE. Decoupling features for diagnosis of reversing and check valve faults in heat pumps. Int J Refrig 2009;32:316–26. https://doi.org/10.1016/j.ijrefrig.2008.05.005.
[53] Mattera CG, Quevedo J, Escobet T, Shaker HR, Jradi M. A method for fault detection and diagnostics in ventilation units using virtual sensors. Sensors 2018;18:3931. https://doi.org/10.3390/s18113931.
[54] Sandin F, Gustafsson J, Eklund R, Delsing J. Basic methods for automated fault detection and energy data validation in existing district heating systems. In: DHC13, the 13th international symposium on district heating and cooling; 2012. p. 182–9.
[55] Gadd H, Werner S. Achieving low return temperatures from district heating substations. Appl Energy 2014;136:59–67. https://doi.org/10.1016/j.apenergy.2014.09.022.

[56] Yliniemi K. Fault detection in district heating substations. 2005.
[57] Sandin F, Gustafsson J, Delsing J. Fault detection with hourly district data. 2013.
[58] Kiluk S. Algorithmic acquisition of diagnostic patterns in district heating billing system. Appl Energy 2012;91:146–55. https://doi.org/10.1016/j.apenergy.2011.09.023.
[59] Månsson S, Davidsson K, Lauenburg P, Thern M. Automated statistical methods for fault detection in district heating customer installations. Energies 2019;12:1–18. https://doi.org/10.3390/en12010113.
[60] Brès A, Johansson C, Geyer R, Leoni P, Sjögren J. Coupled building and system simulations for detection and diagnosis of high district heating return temperatures. Build Simulat Conf Proc 2019;3:1874–81. https://doi.org/10.26868/25222708.2019.210629.
[61] Kane M, Sharma K. Data-driven modeling of adaptive occupant thermostat behavior dynamics. In: 2020 ASHRAE virtual conference; 2020.
[62] Stopps H, Touchie MF. Residential smart thermostat use: an exploration of thermostat programming, environmental attitudes, and the influence of smart controls on energy savings. Energy Build 2021;238:110834. https://doi.org/10.1016/j.enbuild.2021.110834.
[63] Huchuk B, O'Brien W, Sanner S. A longitudinal study of thermostat behaviors based on climate, seasonal, and energy price considerations using connected thermostat data. Build Environ 2018;139:199–210. https://doi.org/10.1016/J.BUILDENV.2018.05.003.
[64] Huchuk B, O'Brien W, Sanner S. Exploring smart thermostat users' schedule override behaviors and the energy consequences. Sci Technol Built Environ 2020;27(2):195–210. https://doi.org/10.1016/j.jss.2012.12.052.
[65] Christensen MH, Li R, Pinson P. Demand side management of heat in smart homes: living-lab experiments. Energy 2020;195. https://doi.org/10.1016/j.energy.2020.116993.
[66] Santos AQ, Jørgensen BN. Control strategies and algorithms for obtaining Energy Flexibility in buildings. 2019.
[67] Stopps H, Huchuk B, Touchie MF, O'Brien W. Is anyone home? A critical review of occupant-centric smart HVAC controls implementations in residential buildings. Build Environ 2021;187:107369. https://doi.org/10.1016/j.buildenv.2020.107369.
[68] Lou R, Hallinan KP, Huang K, Reissman T. Smart wifi thermostat-enabled thermal comfort control in residences. Sustainability 2020;12:1919. https://doi.org/10.3390/su12051919.
[69] Systèmes Dassault. DYMOLA systems engineering. 2006. n.d, https://www.3ds.com/products-services/catia/products/dymola/. [Accessed 26 April 2021].
[70] Klare ABB. Fordele for forbrugere og samfund ved at integrere smarte boliger i energisystemet [Integrating smart dwellings in the energy system presents clear advantages for consumers and society. 2019. https://new.abb.com/news/da/detail/36455/klare-fordele-for-forbrugere-og-samfund-ved-at-integrere-smarte-boliger-i-energisystemet. [Accessed 26 May 2021]. accessed.
[71] Babiak J, Olesen BW, Petrás D. Low temperature heating and high temperature cooling - REHVA guidebook N, vol. 7; 2013.
[72] Dinesen. Instructions before installation. 2014.
[73] Lawrence Berkeley National Laboratory. Modelica Buildings Library - Radiant Slabs n.d. https://simulationresearch.lbl.gov/modelica/releases/latest/help/Buildings_Fluid_HeatExchangers_RadiantSlabs.html.
[74] MAP FMI. Functional mock-up unit (FMI). https://fmi-standard.org/. [Accessed 5 October 2020].
[75] Arendt K, Jradi M, Wetter M, Veje CT. ModestPy: an open-source Python tool for parameter estimation in functional mock-up units. Proc 1st Am Model Conf 2018;154:121–30. https://doi.org/10.3384/ecp18154121.
[76] Videncenter for energibesparelser i bygninger. Indregulering af varmeanlæg i parcelhuse og andre mindre bygninger [Balancing of heating installations in detached houses and other small buildings. 2011.
[77] Cholewa T, Balen I, Siuta-Olcha A. On the influence of local and zonal hydraulic balancing of heating system on energy savings in existing buildings – long term experimental research. Energy Build 2018;179:156–64. https://doi.org/10.1016/j.enbuild.2018.09.009.
[78] Videncenter for energibesparelser i bygninger. Guide - varmeafgiversystemer [Heating emitting systems. 2011.
[79] Danfoss. Gulvvarme - beregningsværktøjer [Floor heating - calculation tools] (accessed March 1, 2021), https://www.danfoss.com/da-dk/service-and-support/downloads/dhs/floor-heating-preset-calculation/#tab-overview; 2021.
[80] Hebenstreit B, Schnetzinger R, Ohnmacht R, Höftberger E, Haslinger W. Efficiency optimization of biomass boilers by a combined condensation - heat pump - system. ECOS; 2011.